Accepted Manuscript

Response of pultruded composite tubes subjected to dynamic and impulsive axial loading

D. Kakogiannis, S. Chung Kim Yuen, S. Palanivelu, D. Van Hemelrijck, W. Van Paepegem, J. Wastiels, J. Vantomme, G.N. Nurick

Please cite this article as: Kakogiannis, D., Chung Kim Yuen, S., Palanivelu, S., Van Hemelrijck, D., Van Paepegem, W., Wastiels, J., Vantomme, J., Nurick, G.N., Response of pultruded composite tubes subjected to dynamic and impulsive axial loading, *Composites: Part B* (2013), doi: http://dx.doi.org/10.1016/j.compositesb.2013.07.022

Response of pultruded composite tubes subjected to dynamic and impulsive axial loading

D. Kakogiannis[a,b,*], S. Chung Kim Yuen[c], S. Palanivelu[d], D. Van Hemelrijck[b], W. Van Paepegem[d], J. Wastiels[b], J. Vantomme[a], G. N. Nurick[c]

[a]*Civil and Materials Engineering Department, Royal Military Academy Renaissancelaan 30, B-1000, Brussels, Belgium*
[b]*Department of Mechanics of Materials and Constructions,Vrije Universiteit Brussel Pleinlaan 2, B-1050 Brussels, Belgium*
[c] *Blast Impact and Survivability Research Unit (BISRU), Department of Mechanical Engineering, University of Cape Town, Private Bag, Rondebosch 7701, South Africa*
[d]*Department of Materials Science and Engineering, Ghent University Sint Pietersnieuwstraat 41, 9000 Gent, Belgium*

Abstract

The energy absorption of circular pultruded composite tubes subjected to axial crush load, transmitted by a small attached mass accelerated by means of an explosive load is presented in this paper. Different masses of explosive are used to provide a range of transmitted impulse and crushed distance of the pultruded composite tubes. The influence of the mass of the explosive on the tube response is investigated with regard to crushed distance, the average crushing force and the specific energy absorption (SEA). The crushing distance increases with increasing transmitted impulse. The results and failure mode are also compared with compression tests carried out on a servo-hydraulic machine (type: MTS-309).

Keywords: A. Glass fibres; B. Impact behaviour; C. Finite element analysis (FEA); D. Pultrusion; Blast loading

1. Introduction

Composite structures such as plates, shells, tubes, stiffeners and stiffened sandwich panels are used in numerous applications due to superior specific energy absorption (SEA)

---

[*]Corresponding author. Tel.:+32 2 742 64 22
Email address: dkakogia@rma.ac.be (D. Kakogiannis)

to weight ratio compared to metallic structures[2, 23]. When subjected to an axial load, a typical composite tubular structure exhibits numerous damage mechanisms such as delamination, matrix cracking, fiber cracking and debonding of the fibers. These failure characteristics of composite tubular structure render them as suitable candidates for high energy absorption applications because of the failure mechanisms that absorb energy, in a highly effective way, during impact events [2, 3].

The most dominant failure mechanism of composite tubes and sections under compressive loading are plastic microbuckling and microcracking [4]. These mechanisms depend on the mechanical properties of the matrix and the fibers [5]. Farley et al. [6] define the different collapse modes: transverse shearing, lamina bending and local buckling.

Apart from the material properties, failure also depends on the geometry of the tube, on loading and boundary conditions. Studies have shown that cylindrical sections are more effective to absorb energy during failure in comparison with square tubes [7, 8]. The aforementioned failure modes (transverse shearing, lamina bending and local buckling) affect the energy absorption capacity of the tube [9]. The energy absorption capacity can be predicted in function of the strain energy release rate and the maximum failure strain for inter-laminar crack growth as presented by Farley et al. [10, 11].

In an axial crash scenario it is essential that most of the kinetic energy in the system is absorbed in such a way that the fiber reinforced tube collapses axially with constant deceleration for an optimum energy absorbing system. The collapse process is often initiated at one end of the tube by a trigger mechanism to reduce the initial peak crush force and to control the crush process [8, 12]. Chung Kim Yuen and Nurick [13] presented an overview of the energy absorbing characteristics of tubular structures with geometric and material modifications. Extensive studies have been carried out on the bevel trigger and tulip triggering mechanism showing that for square sections, with tulip triggering, the crushing is more controllable and predictable and more energy per unit mass is absorbed [14–17]. Thornton [18] reported that for reinforced uni-directionally polyvinylester and polyester matrix circular tubes, during axial compression at high strain rates, a tulip trigger demonstrates a more stable crush and the crushing force is fairly constant in comparison with the bevel triggering. The orientation and the amount of the fibers are directly related to the strain rate dependency of the SEA [18]. In terms of fiber

2

orientation, the unidirectionally reinforced tubes show less strain rate sensitivity [18, 19].

Hitherto, most studies have been conducted under quasi-static loading and crushing velocities of up to $15m/s$. For higher crushing velocities, Karagiozova et al [20] carried out experiments and numerical simulations to investigate the response of aluminium tubes (both square and circular in cross-section) subjected to axial impact load transmitted by a small mass accelerated by the detonation of explosive. Impact velocities in the range of 63 to $127m/s$ were obtained. The analysis showed that the average crushing force is influenced by the inertia of the striking mass. Theobald and Nurick [21] also reported on tubular structures subjected to axial blast load. Theobald and Nurick [21] developed a sandwich-type panel using thin-walled tubes between mild-steel plates and characterized the global behavior and performance of the novel lightweight panel by response of the tubular structure under severe blast load conditions. Different numbers of tubes were used. In some cases the tubular structures had trigger mechanisms. The impact velocities of these tubular structures were not reported. However, after optimization of the placement and thickness of the tubular structures, the panel was a good absorber under severe loading condition.

In the present study the response and failure of pultruded composite tubes subjected to axial dynamic and impact load is investigated. Two different diameters are used with a tulip triggering of two different angles. The SEA and crushing force are compared between dynamic and impulsive loading. A finite element model is created to calculate the crushing force vs time under impulsive loading. The experimental results from the dynamic loading of the tubes are used to calibrate the material model for the finite element calculations. A comparison is made between numerical and experimental results under impulsive loading. The goal of the study is to evaluate the crashworthiness of the examined pultruded composite tubes under impulsive loading.

2. Experimental Setup

2.1. Specimen

The specimens used are cylindrical pultruded composite tubes made of vinylester matrix reinforced with E-glass fibers. The main orientation of the fibers is unidirectional along the tube axis. There are also two layers in the tube wall: one crosswind in $0.5mm$

3

of the thickness, measuring from the inner diameter, and one glass fiber mat on the outer surface of the tube to hold the unidirectional glass fibers during the pultrusion process. The section of the tube with the different groups of fibers is shown in Fig. 1.
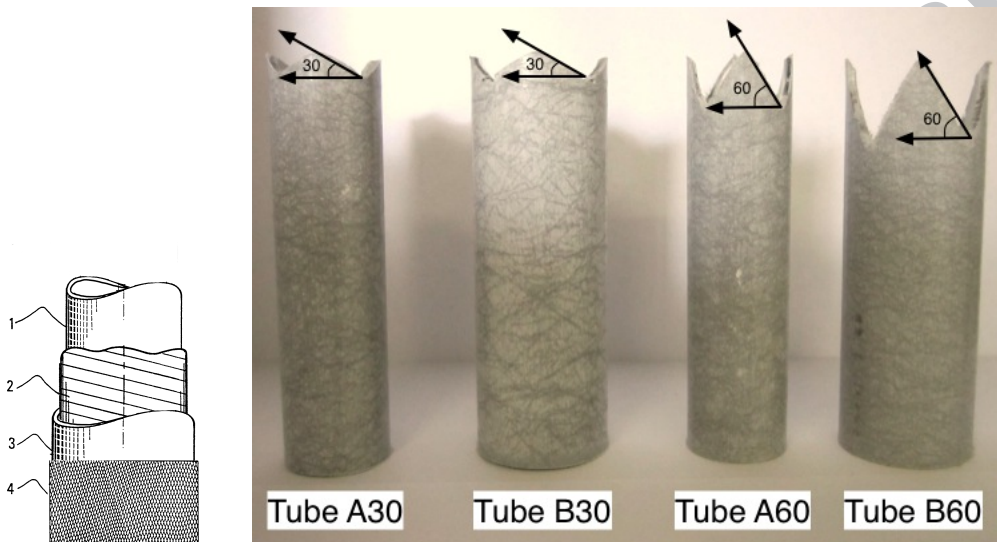
(a) The groups of glass fibers: 1. Unidirectional, 2. Crosswind, 3. Unidirectional, 4. Glass strand mat

(b) The tubular specimens with the tulip triggering of 30 and 60 degrees.

Figure 1: The examined specimens

The tubes are $100mm$ in length and have a wall thickness of $2mm$. Two different outer tube diameters $23mm$ and $30mm$ indicated as tube A and tube B respectively are investigated. All the specimens have a tulip type trigger on the impact end. For tubes A (outer diameter $23mm$) and B (outer diameter $30mm$) two different angles of tulip triggering are used; 30° and 60°. The mass per length is $0.21kg/m$ for tube A 30 , $0.20kg/m$ for tube A 60, $0.32kg/m$ for tube B 30 and $0.30kg/m$ for tube B 60.

2.2. Dynamic compression-dynamic loading

The specimens are crushed axially using a servo-hydraulic machine (type: MTS-309) at a speed of $1000mm/min$ to obtain typical crush force displacement characteristics. The maximum load capacity of the machine piston in tension or compression is $100kN$.

4

For each tube geometry the dynamic compression test is carried out three times for repeatability of experimental results. The specific energy absorption(SEA) is considered to be equal to the energy absorbed by the tube divided by the crushed mass. The energy absorbed is equal to the area under the force displacement graph. If m_l is the mass per meter of the tube and s_f the maximum crushed distance, then:

The energy absorbed is calculated by:

$$E_d = \int_0^{s_f} F(s)\,\mathrm{d}s. \tag{1}$$

And the SEA is calculated by:

$$SEA = \frac{E_d}{m_l s_f} \tag{2}$$

2.2.1. Results

The tubes are crushed up to $50mm$ to obtain the average crushing force of the tube. The average values obtained are shown in Table 1.
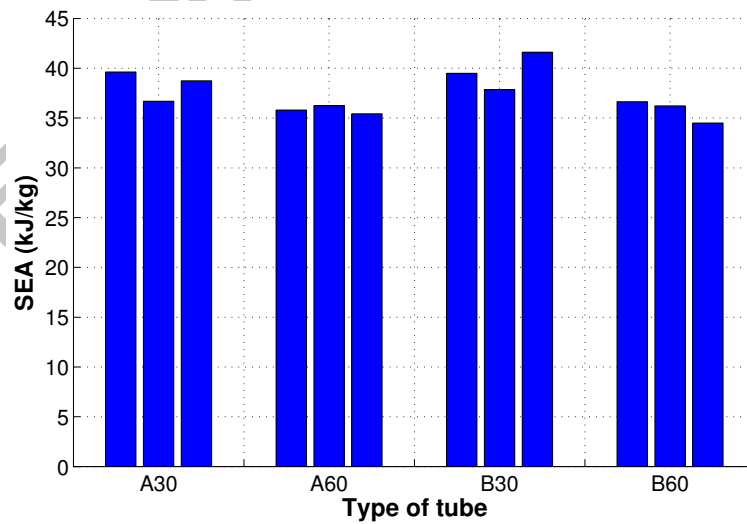
Table 1: Dynamic compression results

Specimen	Average force(kN)	SEA(kJ/kg)
Tube A 30	8	38.34
Tube A 60	8	35.81
Tube B 30	13	39.64
Tube B 60	14	35.77

The curves presented in Fig. 2 show the force vs displacement and SEA (Specific Energy Absorption) for each specimen. For all tubes the tulip triggering creates a stable crushing zone and as the crushing zone advances the force increases. Once the crushing zone has consumed the triggering length, the crushing force reaches a maximum and it is stabilized. In both tubes A and B the triggering angle influences the rising slope of the force vs displacement diagram; for the 30° triggering the maximum crushing force is reached faster in comparison with the 60° triggering due to the trigger length difference between the two different triggering angles. As a result the triggering angle has an effect on the SEA, since the area under the curve is affected, but not on the peak force. The

5

average crushing force is similar for the same crushing distance. The crushing force required for tube B is higher in comparison with tube A due to the larger diameter [16].
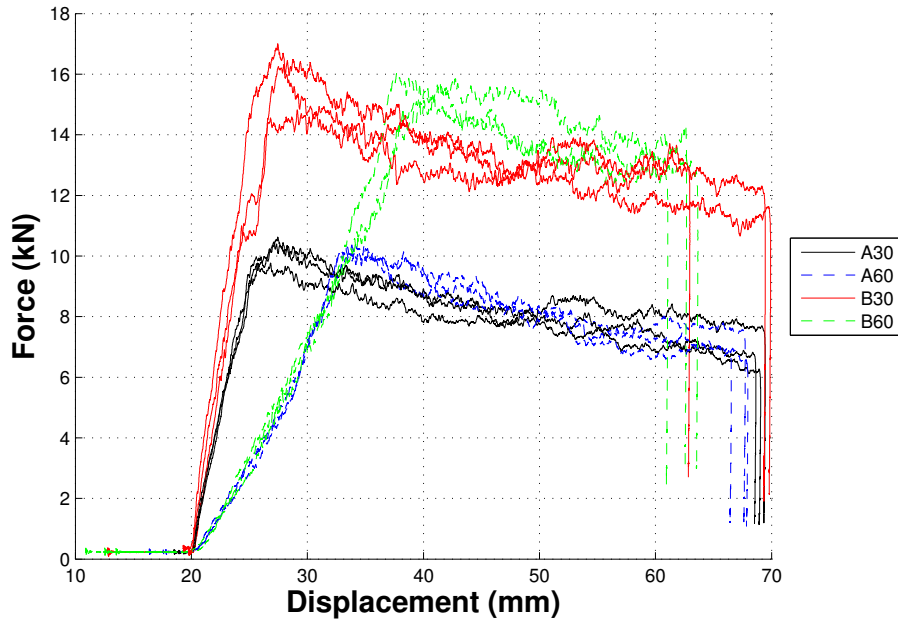
(a) The force vs displacement

(b) The specific energy absorption(SEA)

Figure 2: The results under dynamic compression

6

2.3. Blast tests-impulsive loading

The experimental setup is similar to that used in previous experimental investigations [20, 21]. An impulsive load, created by the detonation of plastic explosive (PE4), is used to accelerate a small mass onto the tubular structure. Three different masses of PE4 (4g, 5g and 6g), cylindrical disc in shape, are used for tubes A 30 and A 60 and 5g for tubes B 30 and B 60. For tube A, the cylindrical disc of PE4 has diameter of 25mm and for tube B the cylindrical disc of PE4 is 30mm in diameter. The explosive charge is evenly spread onto a polystyrene disc, which has a thickness of 13mm and the same diameter of the free striking mass. For tube A, a striking mass of 50mm in diameter weighing nominally 107g is used. For tube B the striking mass used has a diameter of 60mm diameter and is nominally 153g in mass. The striking mass slides freely in an opening in the support plate and in contact with the specimen that is attached on the ballistic pendulum (see Fig.3).

(a) The schematic of the pendulum

(b) The specimen placed on the pendulum
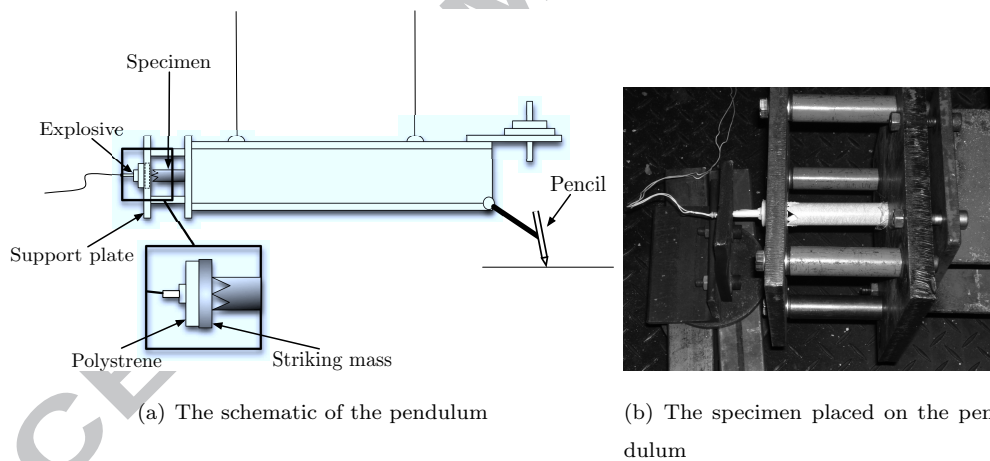
Figure 3: The experimental setup

A detonator taped to 1g of explosive is attached to the centre of the disc of explosive. After the detonation the polystyrene is burnt, the striking mass is accelerated onto the tubular specimen, in an axial direction, causing the specimen to crush. The mass of the explosive is varied by retaining the prescribed diameter but changing the height of the disc of explosive; the aim is to provide a range of crushed distances for the different specimens. The same loading conditions are repeated 4 times for each experiment for

7

repeatability. The impulse imparted onto the specimen is calculated using the swing of the pendulum as performed by [20, 21]. Assuming the conservation of momentum, the initial impact velocity of the striking mass is calculated using the measured impulse:

$$I = MV = mv \Rightarrow v = \frac{MV}{m} \tag{3}$$

Where M is the mass of the pendulum, m is the mass of the striking mass, V is the pendulum velocity and v is the velocity of the striking mass after the detonation. The kinetic energy of the striking mass is assumed to be absorbed by the specimen and is given by:

$$E_{kinetic} = E_{absorbed} = \frac{mv^2}{2} = \frac{(MV)^2}{2m} \tag{4}$$

and the average crushing force:

$$F_a = \frac{E_{absorbed}}{s_f} \tag{5}$$

The crush distance for the tubes is measured by taking the average of four measurements around the circumference every 90°. For each group of tubes charges of three different masses of explosive (4g, 5g and 6g) are used and for the each charge mass, four tests are conducted for the three different groups of tubes: Tube A 30°, Tube A 60°, Tube B 30° and Tube B 60°.

2.3.1. Results

The results are listed in Table 2 and are discussed in the subsequent paragraphs.

2.3.2. Impulse and mass of the explosive

The impulse transmitted onto the specimens is calculated from the swing of the pendulum that has a mass of $71,78kg$. The relation between mass of the explosive and the transmitted impulse is shown in Fig. 4. An increasing linear trend in measured impulse is observed with an increasing mass of explosives with a small variation around the mean value due to experimental variation. The size and mass of the striking mass

8

Table 2: Summary of experimental results

Specimen	Mass of explosive(g)	Impulse(Ns)	Crush distance(mm)	Striking mass velocity(m/s)	SEA(kJ/kg)	Average Force(kN)
Tube A 30	4	8.38	28	78.31	55.8	11.7
Tube A 30	4	8.19	25	76.54	59.7	12.5
Tube A 30	4	7.88	26	73.64	53.1	11.1
Tube A 30	4	7.97	29	74.48	48.7	10.2
Tube A 30	5	8.71	52	81.40	32.5	6.8
Tube A 30	5	9.35	37	87.38	52.6	11.0
Tube A 30	5	9.02	54	84.29	33.5	7.0
Tube A 30	5	9.56	39	89.34	52.1	10.9
Tube A 30	6	11.17	57	101.39	46.7	9.3
Tube A 30	6	10.56	59	98.69	40.7	8.1
Tube A 30	6	11.44	63	106.91	45.8	9.1
Tube A 30	6	10.70	58	100	43.9	8.9
Tube A 60	4	7.74	30	72.33	46.7	9.3
Tube A 60	4	7.47	32	69.81	40.7	8.1
Tube A 60	4	8.16	34	76.26	45.8	9.2
Tube A 60	4	8.11	35	75.79	43.9	8.8
Tube A 60	5	10.09	51	94.29	46.6	9.3
Tube A 60	5	8.95	49	83.64	38.2	7.6
Tube A 60	5	9.89	51	92.42	44.8	8.9
Tube A 60	5	8.95	48	83.64	39.0	7.8
Tube A 60	6	10.23	58	95.60	42.2	8.4
Tube A 60	6	10.91	55	101.96	50.6	10.1
Tube A 60	6	10.36	58	96.82	42.2	8.6
Tube A 60	6	11.86	60	110.84	54.8	11.0
Tube B 30	5	9.77	18	63.85	54.15	17.3
Tube B 30	5	9.15	16	59.80	53.43	17.1
Tube B 30	5	8.75	16	57.18	48.87	15.6
Tube B 30	5	9.51	17	62.15	54.33	17.4
Tube B 60	5	9.49	23	62.02	42.65	12.8
Tube B 60	5	10.32	22	67.45	52.73	15.8
Tube B 60	5	9.02	22	58.95	40.28	12.1
Tube B 60	5	9.15	20	59.80	45.60	13.7

9

m do not appear to influence the measured impulse. The magnitude of the error bar is equal to the standard deviation for each group of all the measurements taken for a specific amount of charge.
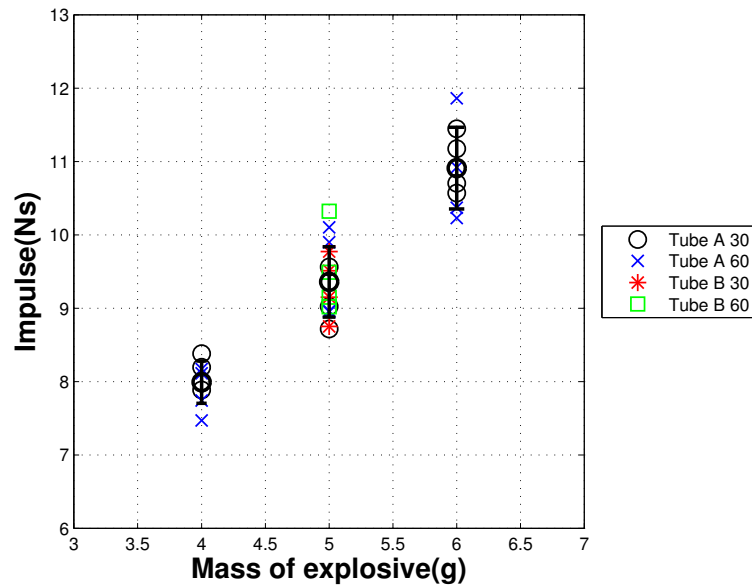

Figure 4: Impulse vs mass of the explosive

2.3.3. Effect of impulse on the crushing distance

The crush distance increases linearly with an increasing transmitted impulse (see Fig. 5) for the range of impulse investigated. For tubes A 30 and A 60 the crush distance is similar for the same impulses. However, it was observed for a charge of 4g of PE4 there is a distinctive difference in crush distance that could be attributed to the length of the triggering in relation to the total crush distance. In the case of Tubes B the crush distance is in general 30% lower in comparison with Tube A. This can be related to the difference in geometry in combination with the increased amount of the material in the section area; as a result, the kinetic energy of the striking mass is absorbed in shorter distance.
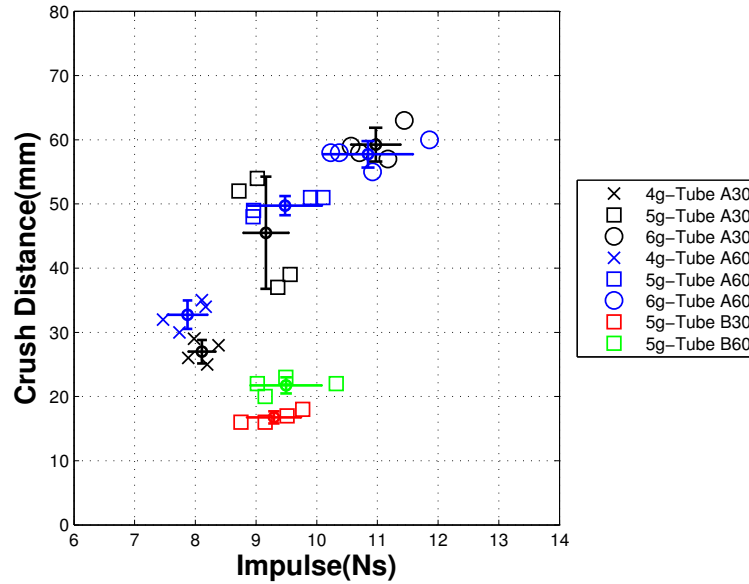
10

Figure 5: Crush distance vs impulse

2.3.4. Effect of impulse on the SEA

The SEA results are shown in Fig. 6. While the impulse is increased the SEA values scatter between $37kJ/kg$ and $55kJ/kg$. A distinctive reduction of the SEA is observed in Tube A 30 whereas in the case of Tube A 60 the SEA does not change with the increase of the charge. Comparing the two triggering angles it is observed that for the lower values of impulse the SEA differs about 18% and for higher impulse values the SEA is the same for both types of triggering. The triggering angle has effect on the SEA of Tube B for a charge of 5g and in terms of geometry the SEA of Tube A is higher in comparison with Tube B for both triggering angles. In general scattering is observed in a lot of measurements and it is created by the irregular crushing due to the boundary conditions; in some experiments the striking mass would impact the specimen obliquely causing asymmetric progressive crushing. Such a specimen that is crushed asymmetrically is shown in Fig. 7 where the irregularly(oblique) crushed tube gave a high impulse reading and as a result the SEA is overestimated.

11

Figure 6: SEA vs impulse

2.3.5. Effect of the mass of the explosive on the average crushing force

The average crushing force was calculated using Eq. 5. Fig. 8 shows the average force required to crush each specimen vs the impulse. The average crushing force of tube A 30 shows a reduction with the increase of impulse from 11kN to 9kN. The force of tube A 60 shows no sensitivity to impulse variations and the average crushing force has a mean value of 9kN. Between tubes A 30 and A 60 a difference observed in the crushing force for a charge of 4g whereas for higher values of impulse the values overlap with a mean value of 9kN. For tube B the crushing force values are higher in comparison with tube A and the maximum crushing force is observed in tube B 30. The results are summarised in Table 3.

3. Comparison of failure pattern between dynamic and impulsive loading

The failure pattern is similar for both types of loading; some fibers bend towards the inner diameter and some towards the outer diameter, the matrix is almost completely fractured and removed, axial cracks are developed between the fibers along the length of the tube and the crosswind fibers are fractured up to the crush front creating a brush

12

Figure 7: Tube A 60 specimens for a charge of 6g. The highlighted specimen is the one crushed assymetricaly in comparison with the rest of the specimens
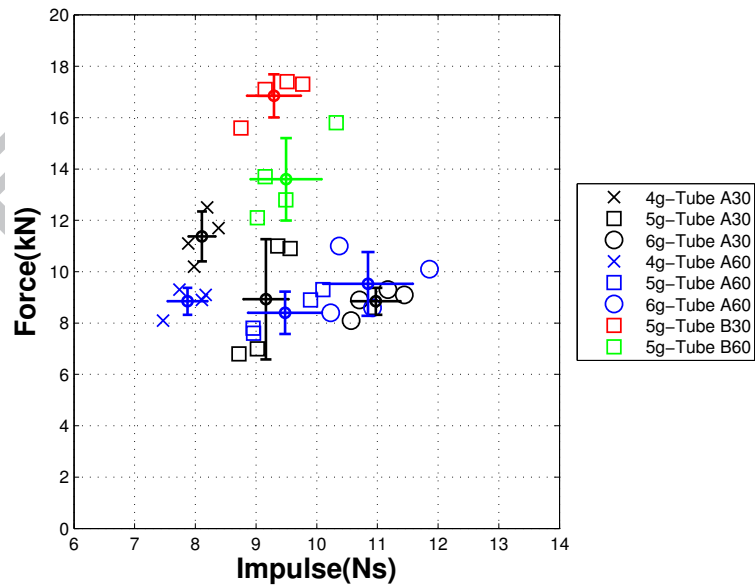

Figure 8: Average crushing force vs impulse

13

Table 3: Variation in impulse and average crushing force

	A30	A60	B30	B60
Mass of explosive (g)	Impulse (Ns)	Impulse (Ns)	Impulse (Ns)	Impulse (Ns)
4	8.10±0.22	7.12±1.77		
5	9.16±0.37	9.47±0.60	9.29±0.44	9.49±0.58
6	10.96±0.49	10.84±0.74		
Mass of explosive (g)	Average Force (kN)	Average Force (kN)	Average Force (kN)	Average Force (kN)
4	11.37±0.97	8.85±0.54		
5	8.92±2.34	8.40±0.82	16.85±0.84	13.60±1.60
6	8.85±0.52	9.52±1.24		

type object (see Fig. 9 and 10).

Figure 9: The specimen failure under dynamic(left) and impulsive(right) loading

During axial compression under the two types of loading, differences are observed in failure. The main difference between dynamic and impulsive loading is the development of the main/principle crack along the section of the tube wall. For the dynamic loading a small wedge from debris is formed on the top of the wall (at the crash front) and the main crack develops in the middle of the wall thickness where the fibers split towards the inner and outer side as illustrated in Fig. 11. In the case of impulsive loading the wedge is developed by crosswind fibers and is bigger in comparison with the wedge created during the dynamic compression. The crack is propagated at the interface between the unidirectional and crosswind fibers as presented in Fig. 12.
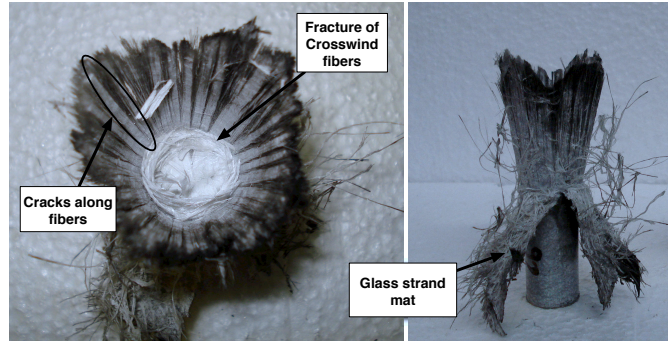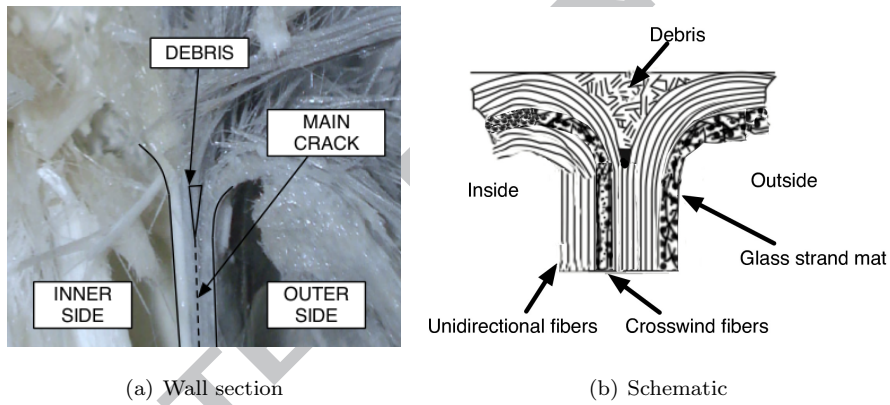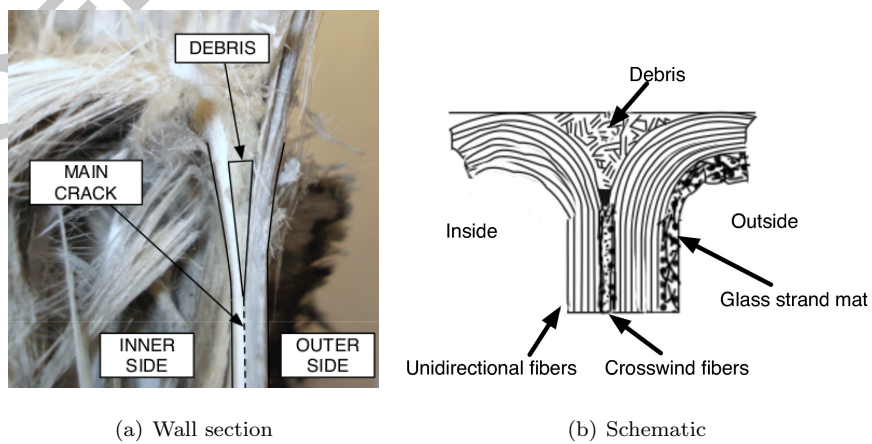
14

Figure 10: The failure pattern under impulsive loading

(a) Wall section   (b) Schematic

Figure 11: The failure under dynamic compression tests

(a) Wall section   (b) Schematic

Figure 12: The failure under impulsive compression tests

15

4. Finite Element Model

Simulations are carried out for the crushing of the tubes A30, A60, B30 and B60 under dynamic and impulsive loading.

4.1. Geometry and Boundary Conditions

The finite element model of the dynamic loading contains only the tubular specimen that is fixed at the bottom and a rigid wall(RIGID_WALL_GEOMETRIC_ FLAT_ MO-TION) is compressing it with a coefficient of friction 0.22 [22] and with the same velocity as in the experiment. The model of the impulsive loading includes the tubular specimen, fixing the bottom nodes, and the striking mass. The striking mass is modeled with solid elements using elastic material model with the properties of steel. The load is applied as a rectangular impulse (force vs time), measured experimentally, with a duration equal to the time required to burn the explosive [20, 23]. The time duration of the impulse is calculated by dividing the radius of the cylindrical explosive by the burning velocity of PE4($8200m/s$).

The tubular specimen is modelled by four layers of shell elements of equal thickness which are considered to be homogeneous. The size of the elements is $0.87mm$ to $1mm$. Even though the tube walls are not composed by layers the main crack could be considered as a type of delamination. The delamination mechanism can be simulated using a tiebreak interface condition between the adjacent layers of the composite shell structure. In the present model between the element layers the tiebreak condition AUTOMATIC_SURFACE _ TO _ SURFACE _ TIEBREAK is used to simulate the main crack that is developed on the tube wall. In the tie-break interface algorithm, two nodes of the model are tied together until the interaction stresses between the two nodes satisfies the following quadratic delamination conditions [24] :

$$\frac{\sigma_z^2}{S_n^2} + \left(\frac{\sigma_{xz}^2 + \sigma_{yz}}{S_s^2}\right) \geq 1 \tag{6}$$

where σ_z is the out of plane normal stress, σ_{yz} and σ_{xz} are the inter-laminar shear stress. S_n is the out of plane normal strength and S_s is the inter-laminar shear strength. In the model the walls in order to split require a tensile stress equal to σ_{yy} or a shear stress equal to τ_{xy} as indicated in table 4. After the separation of the nodes sliding is allowed

16

between the layers. Also a self-contact algorithm is included for simulating the contact between the elements of the same layer. Static and dynamic coefficients of friction are set to values of 0.22 to 0.35 [22].

4.2. Material Model

As already mentioned, the tubes used for the tests are manufactured by a pultrusion process (M/s EXEL, Belgium) and both mechanical and strength properties are not available. Consequently, the properties of the numerical model are estimated by calibrating the finite element model of the dynamic compression tests using, as an initial step, typical values from the literature for pultruded profiles. The elastic properties and the strength properties for a glass-fiber/polyester pultruded profile, as presented in [25], are used as a starting point for the simulations. By repeating the simulations the strength properties are updated in order to match the results up to the limit where the numerical and experimental average crushing force of the dynamic compression are in good agreement. The material model used, for both dynamic and impulsive loading, is MAT 58 from the material library of LS-DYNA, which is based on a continuum damage mechanics model as proposed by Matzenmiller et al. [26]. The MAT 58 factors SLIMxx are used to limit the stress so that the damage value is modified and elastoplastic like behaviour is achieved with the threshold stress. Their values are chosen as recommended by [27]. The failure strains are equal to ϵ_y, calculated from the elastic and strength properties, increased by 10% as illustrated in Fig. 13. The value of 10% is used because a value higher than that leads to elastic bucking instead of progressive crushing and a value lower than 10% gives incorrect values for the crushing force. In the stress strain curve the stress in the elements is increased reaching a maximum value. Due to the SLIMxx factors the stress remains constant until erosion is achieved when strain at failure ϵ_f is reached. The final properties, after the updating procedure, used for the numerical simulation of the pulturded tubes are presented in Table 4.

4.3. Results

The numerical and experimental curves of force vs displacement for the dynamic loading are shown in Fig. 14.
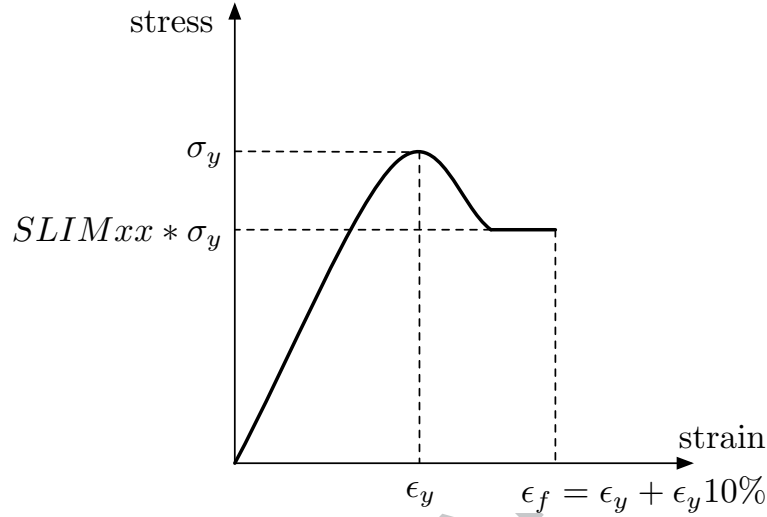
17

Figure 13: Stress-strain curve of MAT 58 where σ_y is the stress from the strength properties of the material.

Table 4: Pultruded tube properties

Elastic Properties				Strength Properties				MAT 58 factors [27]		Failure Strains	
$E_{xxT}(GPa)$	31.2	$E_{xxC}(GPa)$	31.2	$X_T(GPa)$	1.2	$X_C(GPa)$	1.2	SLIMT1	0.05	ϵ_{11T}	0.0423
$E_{yyT}(GPa)$	9.36	$E_{yyC}(GPa)$	9.36	$Y_T(MPa)$	800	$Y_C(GPa)$	1	SLIMC1	1	ϵ_{11C}	0.0423
v_{xy}	0.29							SLIMT2	0.05	ϵ_{22T}	0.1177
v_{yx}	0.1							SLIMC2	1	ϵ_{22C}	0.0940
$G_{xy}(GPa)$	7.33			$S_C(MPa)$	800			SLIMS	1.0e-08	τ_{12}	0.275

The numerical curves follow the same pattern as the experimental; while the crush front proceeds the force increases linearly until the triggering length is consumed, once the rigid wall meets the full section of the tube the crushing force is stabilized at an average crushing value. The average numerical crushing force is in good agreement with the average experimental with the only difference that there are a fluctuations observed in the numerical curve. In all models the tube walls bend outwards in contrast with the experimental failure pattern, the typical crushing process is shown in Fig. 15.

Simulations of impulsive loading give a more accurate failure pattern as shown in Fig. 16 and 17. The striking mass is accelerated by the impulsive load and it crushes the tube until its kinetic energy is reduced to zero. The interior layer bends towards the inner side of the tube an the three others bend outwards creating a crack in the wall

18

(a) Tube A 30

(b) Tube A 60
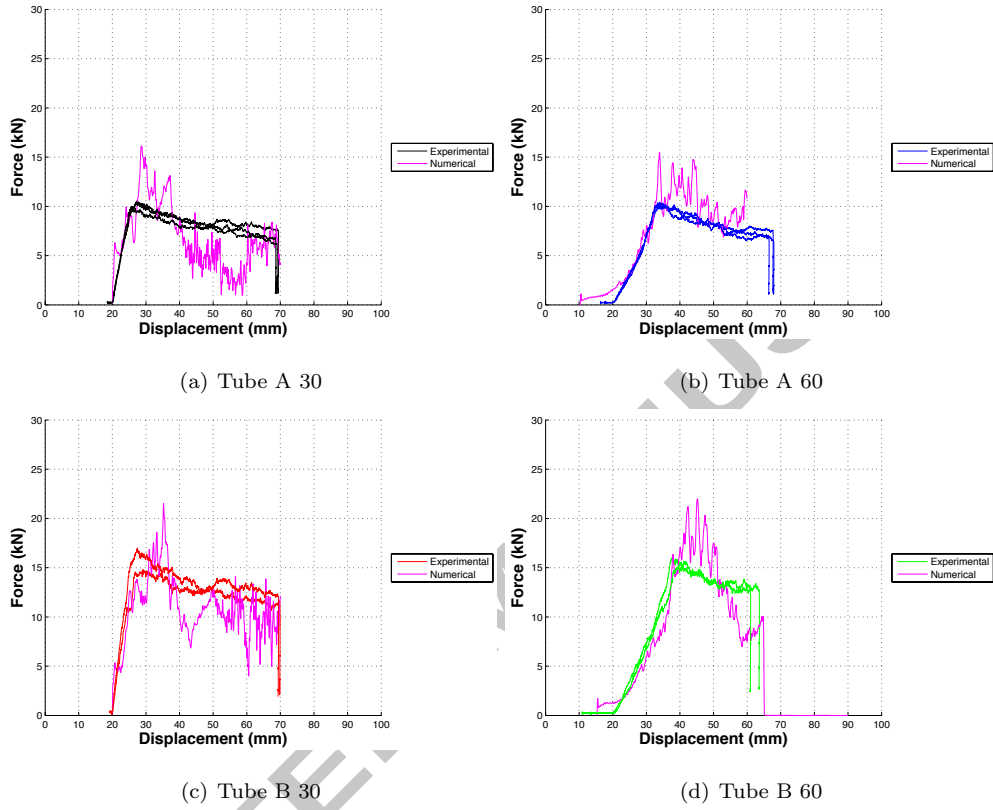
(c) Tube B 30

(d) Tube B 60

Figure 14: Comparison of numerical and experimental force vs displacement curves under dynamic loading.
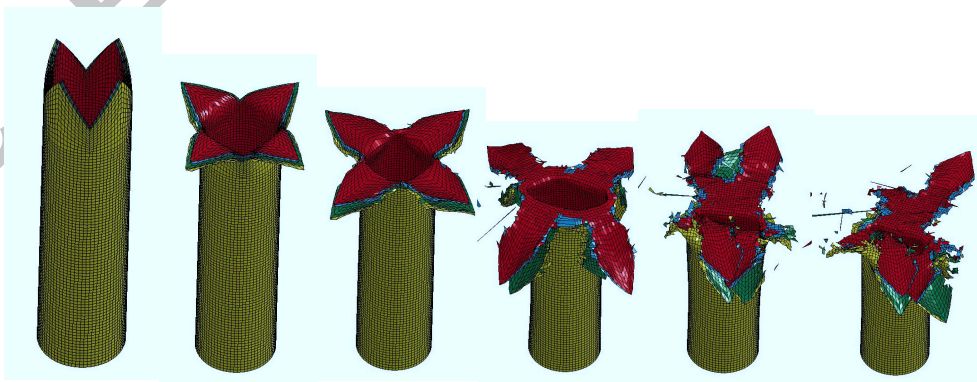

Figure 15: The crushing process modeled under dynamic loading of tube A 60
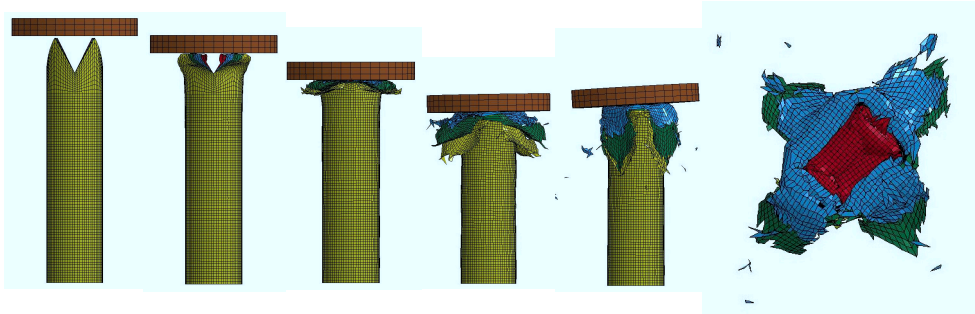
19

Figure 16: The crushing process modeled under impulsive loading of 4g of the A 60
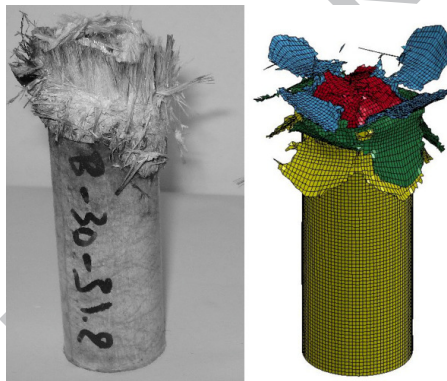
according to the tiebreak condition.

Figure 17: The failure pattern comparison of tube B 30 under impulsive loading

The crushing force between the striking mass and the tube is presented in Fig. 18 in function of the displacement of the striking mass. A force peak is observed in the beginning for $5mm$, the force drops at $5kN$ and then increases until a maximum value until it reduces until the end of the crushing process. The force diagrams for all tubes of 60 degrees has a triangular form in comparison with the triggering of 30 degrees which is more trapezoidal. For tubes A 30 and A 60 the force developed during the crushing process is higher in comparison with the calculated from the experiments and also higher in comparison with the numerical model of the dynamic compression. For tubes B 30 and B 60 the numerical crushing force values are in good agreement with the experimental values. The crushing distance comparison, under impulsive loading, is summarised in Table 5. The numerical crush distance for 60 degrees triggering is higher

20
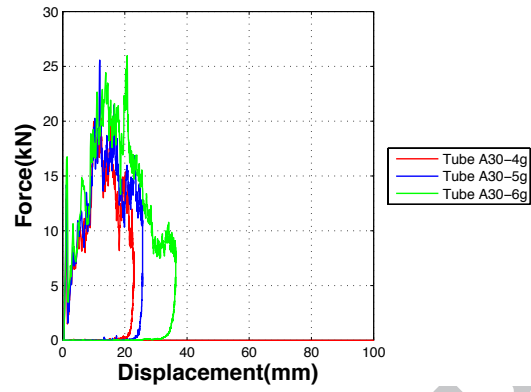
(a) Tube A 30
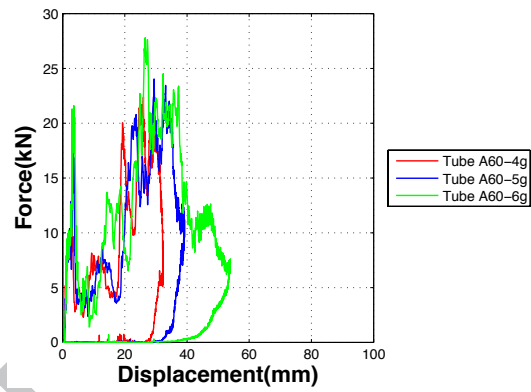
(b) Tube A 60
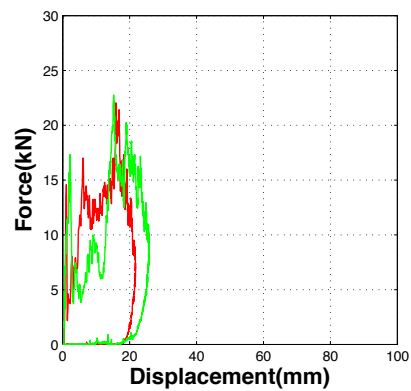
(c) Tube B 30

Figure 18: Force vs striking mass displacement (impulsive loading) resulting from the numerical simulation.

21

in comparison with the 30 degrees triggering for both tubes A and B, as observed in the experiments. Also by increasing the impulsive load the crush distance increases. Numerical crush distance is lower in comparison with experimental for tubes A 30 and A 60 for all charges and the best convergence is observed for tube B 30 and B 60.

Table 5: Experimental and numerical crush distance for impulsive loading

Specimen	Mass of explosive(g)	Average Experimental crush distance(mm)	Numerical crush distance(mm)
Tube A 30	4	27±1.82	22.8
Tube A 30	5	45.5±8.73	25.7
Tube A 30	6	59.25±2.63	36.4
Tube A 60	4	32.75±2.21	32.3
Tube A 60	5	49.75±1.5	39.2
Tube A 60	6	57.75±2.06	53.7
Tube B 30	5	16.75±0.95	21.7
Tube B 60	5	21.75±1.25	25.8

22

5. Conclusions

The crashworthiness of pultruded composite tubes is studied under dynamic and impulsive loading. The results of the dynamic loading are used to validate a finite element model and compare the numerical results with experimental under impulsive regime. The effect of impulse on the SEA, the crush distance and the crushing force is investigated taking into account the influence of the triggering angle mechanism for three tubular diameters.

Under dynamic loading conditions, the triggering angle affects the SEA but not the average crushing force. The 30 degree triggering tubes have higher SEA and the increase in the force is less gradual in comparison with the 60 degree triggering. Under impulsive loading conditions, the relation between the mass of the explosive and the impulse is linear and also the maximum crush distance is increased linearly with the increase of impulse for the examined range of charges. The triggering angle seems to have an effect on the crushing distance for the charge of $4g$ for tube A and $5g$ for tube B. On tube A, for higher charges, there is no effect of the triggering angle on the crush distance. The same effect is observed for the SEA and crushing force values; for lower charges the SEA and the crushing force is higher for the 30 degree triggering and when the impulse increases there is no difference observed between the examined triggering angles.

Comparing the dynamic and impulsive loading it is observed that for all tubes the SEA is increased under impulsive regime and the crushing force developed at the crush front is also increased. A significant difference is observed in the failure pattern and more specifically on the main crack developed in the tube wall. In the case of the dynamic loading the main crack develops in the middle of the wall thickness and in the case of impulsive loading it develops in the layer of the crosswind fibers for all types of tubes, so the variations along the thickness could have an effect on the failure pattern under impulsive loading but further experimental work needs to be conducted.

In all values, under impulsive loading, scattering is observed that can be attributed to the complexity of a blast load and the anisotropy of the composite specimens. Also the non-uniform crush of the specimens, that were crushed obliquely, influence the swing of the pendulum and the calculated values depending on the maximum displacement of the pendulum. By increasing the diameter of the specimen it is observed that the SEA

23

does not increase significantly and higher average force is required during crushing.

Conclusively, tube A 30 seems to be the most suitable energy absorber for the specific range of loads due to the reason that the average force required to crush is relatively low and gives high SEA values for all charges. For dynamic compression the 30° tubes absorb more energy so the higher the angle the more suitable is the tube for energy absorption application.

Axial tube crush simulations were carried out for dynamic and impulsive loading. The attempt to calibrate manually the parameters of MAT 58 was successful only for the case of tubes with 60 degrees triggering since the numerical crush distance was closer to experimental. Even though tube A 30 was indicated as the best energy absorber by the finite element model, the values of crush distance were significantly underestimated. The overall comparison between experimental and numerical results leads to the observation that an optimisation method could be used to investigate further the effect of each parameter of the specific material model for dynamic and impulsive loading. Finally, further efforts need to be invested towards the numerical modeling of pultruded tubes in order to simulate in detail the mechanisms of failure that absorb energy during crushing.

Acknowledgements

References

[23] P. S. Bulson, Explosive Loading of Engineering Structures, E and FN Spon (1997).

[2] A. A. A. Alghamdi, Collapsible impact energy absorbers: an overview, Thin-Walled Structures, Volume 39 (2001), 189-213.

[3] G. Lu and T. Yu, Energy Absorption of Structures and Materials, Woodhead Publishing Limited (2003), 144-173.

[4] P. M. Jelf and N. A. Fleck, Compression Failure Mechanisms in Unidirectional Composites, Journal of Composite Materials, Volume 26, (1992), 2706-2726.

[5] D. W. Schmueser and L. E. Wickliffe, Impact Energy Absorption of Continuous Fiber Composite Tubes, Journal of Engineering Materials and Technology, Volume 109 (1987), 72-77.

[6] G. L. Farley and R. M. Jones, Crushing characteristics of continuous fibre-reinforced composite tubes, Journal of Composite Materials, Volume 26 (1992), 37-50.

24

[7] P. H. Thornton and P. J. Edwards. Energy absorption in composite tubes. Journal of Composite Materials, Volume 16 (1982), 521-545.

[8] S. Palanivelu, W. Van Paepegem, J. Degrieck, J. Van Ackeren, D. Kakogiannis, D. Van Hemelrijck, J. Wastiels, J. Vantomme, Experimental study on the axial crushing behaviour of pultruded composite tubes, Polymer Testing, Volume 29 (2010), 224-234.

[9] D. Hull, A Unified Approach to Progressive Crushing of Fibre-Reinforced Composite Tubes, Composites Science and Technology, Volume 40 (1991), 377-421.

[10] G. L. Farley, Energy absorption in composite materials for crashworthy structures, Sixth International Conference on Composite Materials and Second European Conference on Composite Materials: ICCM-VI (1987), 3.57-3.66.

[11] G. L. Farley and R. M. Jones, Prediction of the energy-absorption capability of composite tubes, Journal of Composite Materials, Volume 26 (1992), 388-404.

[12] H. G. S. J. Thuis and V. H. Metz. The influence of trigger configurations and laminate lay-up on the failure mode of composite crush cylinders, Composite Structures, Volume 28 (1994), 131-137.

[13] S. Chung Kim Yuen and G. N. Nurick, The energy absorbing characteristics of tubular structures with geometric and material modifications: an overview, Applied Mechanics Reviews, Volume 61 (2008). 020802 (15 pages)

[14] M. J. Czaplicki and R. E. Robertson, Comparison of bevel and tulip triggered pultruded tubes for energy absorption, Composites Science And Technology, Volume 40 (1991), 31-46.

[15] M. A. Jimenez, A. Miravete, E. Larrode, D. Revuelta, Effect of trigger geometry on energy absorption in composite profiles, Composite Structures, Volume 48 (2000), 107-111.

[16] P.H. Thornton, Effect of trigger geometry on energy absorption in composite tubes, Fifth International Conference on Composite Materials: ICCM-V (1985), 1183-1199.

[17] P. H. Thornton. The crush behavior of glass fiber reinforced plastic sections. Composites Science and Technology, Volume 27 (1986), 199-223.

[18] P. H. Thorton, The Crush behavior of pultruded tubes at high strain rates, Journal of Composite Materials, Volume 24 (1990), 594-615.

[19] G. L. Farley, The effects of crushing speed on the energy-absorption capability of composite tubes, Journal of Composite Materials, Volume 25 (1991), 1314-1329.

[20] D. Karagiozova, G. N. Nurick, S. Chung Kim Yuen, Energy absorption of aluminium alloy circular and square tubes under an axial explosive load, Thin-Walled Structures, Volume 43 (2005), 956-982.

[21] M. D. Theobald and G. N. Nurick Numerical investigation of the response of sandwich-type panels using thin-walled tubes subject to blast loads, International Journal of Impact Engineering, Volume 34 (2007), 134-156.

[22] C. J. McGregor, R. Vaziri, A. Poursartip, X. Xiao, Simulation of progressive damage development in braided composite tubes under axial compression, Composites Part A: Applied Science and Manufacturing, Volume 38 (2007), 22472259.

[23] P. S. Bulson, Explosive Loading of Engineering Structures, E & FN Spon, 1997.

[24] D. A. Kakogiannis, D. Van Hemelrijck, J. Wastiels, J. Van Ackeren, S. Palanivelu, W. Van

25

Paepegem, J. Vantomme, G. N. Nurick, S. Chung Kim Yuen, Experimental and numerical study of the energy absorption capacity of pultruded tubes under blast load. Society for Experimental Mechanics - SEM Annual Conference and Exposition on Experimental and Applied Mechanics, Volume 3 (2009), 2091-2098.

[25] G. D. Sims and W. R. Broughton, Comprehensive Composite Materials, Volume 2 (2000), 151-197.

[26] A. Matzenmiller, J. Lubliner, R.L. Taylor, A constitutive model for anisotropic damage in fiber-composites, Mechanics of Materials, Volume 20 (1995), 125-152.

[27] LS-DYNA Keyword User's Manual, Volume II : Material Models Version 971, Livermore Software Technology Corporation (LSTC) May 2007.